20th International Congress on Sound & Vibration

ICSV20
Bangkok,Thailand
7-11 July 2013

THE EXPERIMENTAL RESPONSE OF A BROADBAND BASE-EXCITED VIBRATION ISOLATOR INCORPORATING CUBIC DAMPING

Nuttarut Pananda, Neil S. Ferguson and Timothy P. Waters

Institute of Sound and Vibration Research (ISVR), University of Southampton, SO16 3HF, UK.

e-mail: np2g09@soton.ac.uk

Structural damping is often assumed to be viscous and linear which leads to comparatively straightforward vibration analysis. In the case of vibration isolation mounts this assumption of linearity is particularly questionable and one might want to know the effect of a nonlinear damping characteristic on the isolation performance. This paper considers the isolation performance of a single degree of freedom system with cubic damping. Previous work has considered the case of harmonic base excitation in which cubic damping is less favourable than linear damping. This work is summarised briefly here and extended to random base motion. The study is predominantly experimental in which cubic damping is realised using simple velocity feedback control. The rig is first described and characterised in its passive state prior to implementing linear and cubic velocity feedback. It is found that, unlike the case of harmonic base excitation, cubic damping offers very similar performance to linear damping. The reason for this difference in behaviour is identified by considering the probability density functions of the response variables.

1. Introduction

A distinctive characteristic of vibration isolation is that damping is beneficial for suppressing rigid body mount resonances but detrimental in the frequency range for which the isolation system is principally designed. This inherent trade-off is well understood for the case of linear viscous damping. One might expect a trade-off also to exist when damping is nonlinear and it is an interesting question as to whether an increase in nonlinear damping more or less compromises the performance than in the linear case. An additional issue for the nonlinearly damped system is that force and motion transmissibilities differ, since reciprocity does not hold, and therefore need to be addressed separately.

Vibration isolation systems incorporating cubic or higher order anti-symmetric damping have been a topic of interest in recent years[1-3]. In particular, it has been reported that cubic damping can be used to good effect to suppress resonance without any significant detriment at high frequencies in the case of force transmissibility. This is explicable physically since the relative velocity across the damper is high at resonance and low at high frequencies. This is not true of base excited systems and cubic damping has been reported to be detrimental for both shock[4] and harmonic excitation[5,6]. Theoretical comparisons between force and base excited isolation systems have also been in reported[7,8] and show displacement transmissibility rising towards unity at high frequencies. The theoretical results for discrete frequency harmonic excitation have been validated experimentally[9].

Another consequence of system nonlinearity is that the estimated transfer functions for steady state vibration depend on the nature of the excitation signal. A random force or base input can be expected to result in a different transmissibility function than for harmonic excitation, or indeed a random input with a different spectrum. The purpose of this paper is to consider motion transmissibility for a base excited system subject to a random input for which a band-limited random signal is chosen.

This paper begins in section 2 by summarising briefly the isolation performance of a single degree-of-freedom (SDOF) system with cubic damping subjected to harmonic excitation which serves as a benchmark case. Section 3 describes a rig that has been designed to behave as a SDOF system with cubic damping which is realised by velocity feedback. Experimental results are presented in section 4 for the case of random base excitation. These results are profoundly different from those due to harmonic excitation. Numerical simulations are presented in section 5 and analysed to gain some insight into the cause of the differing behaviours.

2. Theoretical analysis and response prediction methods

The theoretical model used in this study is that of a SDOF system subject to base excitation as shown in Fig. 1 (a). The isolator spring is assumed to be linear but acting in parallel with a nonlinear damping component comprising both linear and cubic viscous damping terms. Fig. 1 (b) shows the damping characteristics for both. The equation of motion for the system is given by

$$m\ddot{x} + c_1\left(\dot{x} - \dot{x}_0\right) + c_3\left(\dot{x} - \dot{x}_0\right)^3 + k\left(x - x_0\right) = 0 \tag{1}$$

where x and x_0 represent motions of the isolated mass and the base, m and k are the mass and isolator stiffness, and c_1 and c_3 are the linear and cubic damping coefficients respectively. The undamped natural frequency is given by $\omega_n = \sqrt{k/m}$.

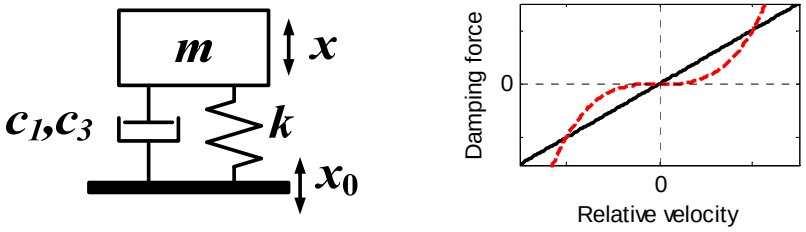

(a) (b)

Figure 1. (a) A single degree of freedom (SDOF) base excited isolation model with a combination of linear viscous c_1 and cubic damping c_3 and linear stiffness k, **(b)** Characteristic diagram for linear viscous damping (**—**) and cubic damping (--).

In previous studies[9], the base excitation was assumed to be time-harmonic, i.e. $x_0 = X_0 \cos(\omega t)$ and the transmissibility of the system was evaluated by considering only the component of the response at the excitation frequency. The ratio of the displacement amplitudes of the mass and base are plotted in Fig. 2. These were obtained theoretically using the Harmonic Balance Method and so are approximate, although previously validated by both numerical and experimental means. These plots show that increasing the value of the cubic damping coefficient reduces the response level around resonance but increases the response for excitation frequencies high above resonance. However, the behaviour differs from that of a linearly damped system in a detrimental way in that the amplitude of the response rises at high frequencies and approaches that of the base. The reason for this behaviour can be attributed to the large relative velocity that occurs across the

mount at high frequencies for the base-excited case. The damping force becomes disproportionately high due to the inclusion of the cubic damping term and ultimately acts as a rigid link in the high frequency limit. The purpose of this paper is to extend this previous work to the case of random base excitation.

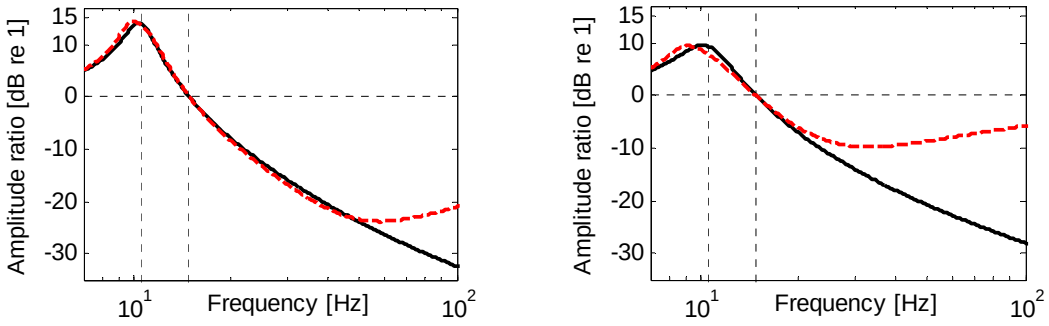

(a) Lower damping (b) Higher damping

Figure 2. The approximate displacement amplitude ratios of the base excitation and the isolated mass for the SDOF base excited isolation system possessing cubic damping subject to discrete harmonic base excitation using Harmonic Balance Method. Linear responses (—) and cubic damping responses (—)

3. The experimental rig

3.1 Rig design and characterisation

An experimental rig was designed to behave as a simple SDOF system that could be base-excited by mounting it on the table of a large electromagnetic shaker, as shown in Fig. 3. A second electrodynamic shaker (LDS model V101) was employed to deliver an active damping force through a velocity feedback control system. The secondary shaker was mounted to an aluminium plate forming a total isolation mass of about 1.5 kg comprising that of the plate and the shaker minus the mass of the shaker's armature. The armature of the shaker was connected to the base by a stinger that can be considered as a rigid link. The isolation mass was thereby supported by the suspension stiffness of the shaker (3.15kN/m) and also two helical springs each of stiffness about 1.00 kN/m. Thus, the total vertical stiffness is about 5.15 kN/m. The natural frequency of the bounce mode was predicted to be 9.32 Hz. The rig was designed to ensure that the pitch mode, whilst not deliberately excited, occurred at a much lower frequency of about 3 Hz.

The displacement amplitude ratio for the passive system is shown in Fig. 4. Note that the amplitude ratio is identically the transmissibility ratio since the system is linear in this configuration. The data are in close agreement with the expected response of a linear SDOF system except below 5 Hz, where excitation of the system is inadequate, and also approaching 200Hz where the internal resonances of the helical springs are expected to and indeed do occur. With this in mind the frequency range of interest was chosen to be 7-100 Hz.

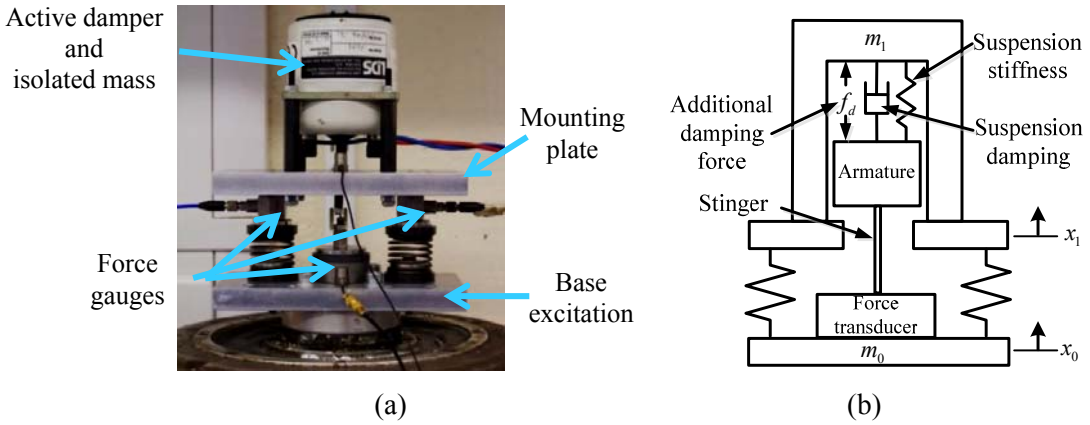

Figure 3. The experimental rig to represent a SDOF base excited isolation system. (a) photograph of assembly and (b) dynamic model of the rig

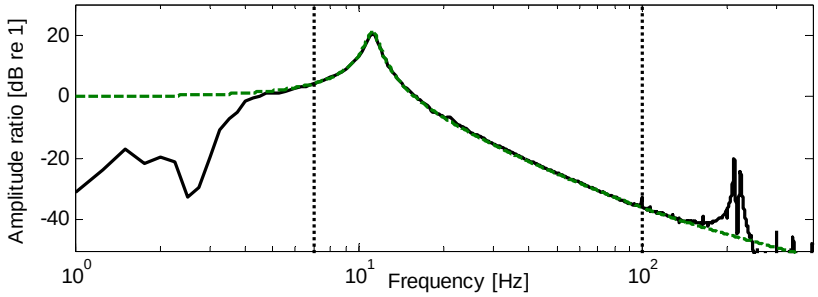

Figure 4. Displacement amplitude ratio of the SDOF base excited isolation system subject to broadband random input with no damping control; experimental results (—) and fit to the data using a SDOF linearly damped model (--)

3.2 Implementation of active damping

The secondary actuator described in the previous section enables active damping to be implemented via velocity feedback control in addition to the passive damping inherent in the rig. A block diagram of the control system is shown in Fig. 5. The velocity signals of the base excitation and isolated mass were obtained from the charge amplifiers which integrated the acquired acceleration signals. The relative velocity was calculated within the control unit. The control unit has the ability to process an arbitrary damping configuration, but in this instance linear and cubic damping configurations were considered. The data processing unit sampled the signal digitally at a sample rate of 6 kHz. As a result, there was no effect from the delay of the feedback signals in the frequency range of interest, namely 7-100 Hz.

3.3 Broadband base excitation

The base excitation was defined to be random with a frequency range of 7-100 Hz and constant displacement. The one-sided PSD level was controlled using the LMS Test.Lab 12A Random Control workbook. The level of excitation chosen corresponded to the displacement limit of the active damper. The one-sided velocity PSDs of the base excitation are plotted in Fig. 6. The base excitation PSD level was controlled to be the same for all scenarios.

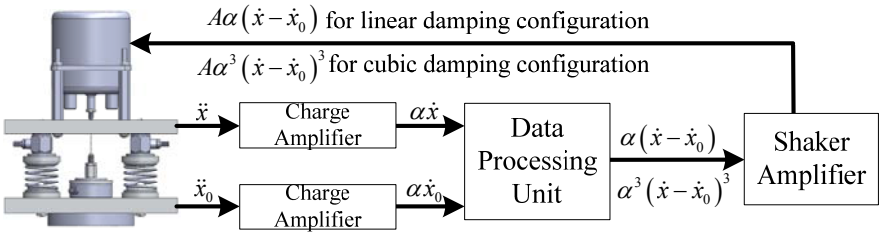

Figure 5. Block diagram of the feedback loop; $\ddot{x}$ and $\ddot{x}_0$ are accelerations of the isolated mass and base input, $\dot{x}$ and $\dot{x}_0$ are the associated velocities, α and A are the gains from the charge amplifier and shaker amplifier respectively.

4. Experimental procedure and results

The rig described in section 3 was used to implement and compare linear damping and cubic damping. To enable meaningful comparisons the amplifier gains (shown as A in Fig. 5) were chosen so as to achieve the same peak value in the amplitude ratio at resonance for the two damping types. The levels chosen resulted in peaks of 15dB and 10dB.

PSDs of the velocity responses were estimated based on 100 averages each of 8 seconds duration. A Hanning window was used with 75% overlap. The PSDs of the isolated mass and base velocities are shown in Fig. 6 for the cases of both linear and cubic damping. The corresponding H_1 estimator of the transfer functions are shown in Fig. 7. The results for the linear and nonlinear systems are very similar which is in stark contrast to the corresponding results for harmonic excitation (see Fig. 2). Fig. 7 also shows the transfer functions obtained from simulations using direct numerical integration of the equations of motion, as described in the following section. These simulations are in close agreement with the measured data.

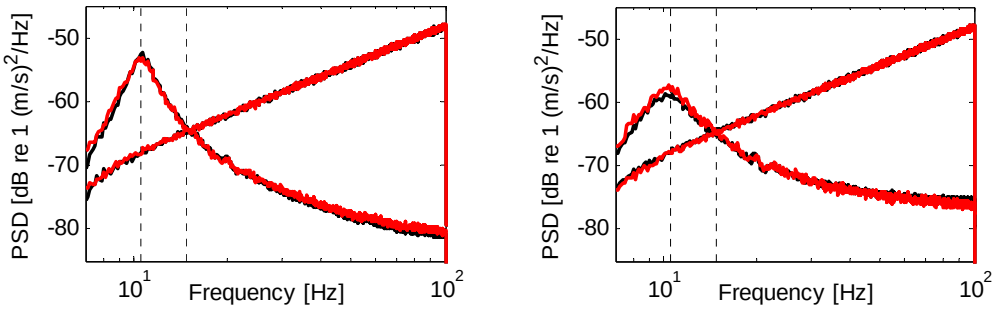

(a) Lower damping (b) Higher damping

Figure 6. Estimated displacement PSD for the base input and the isolated mass linear damping (—) and cubic damping (—)

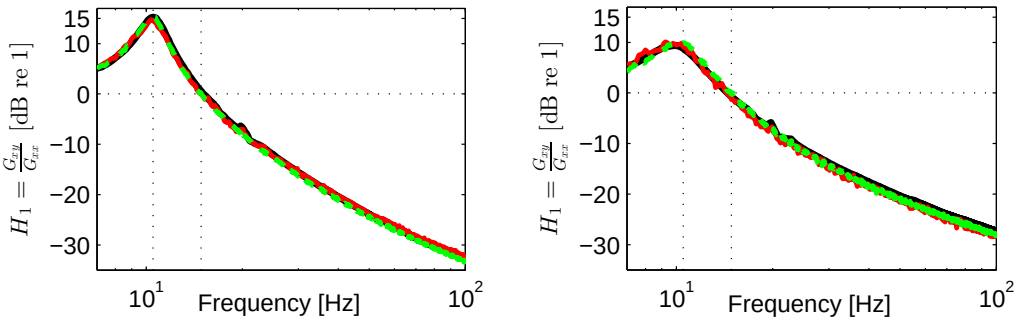

(a) Lower damping (b) Higher damping

Figure 7. H_1 estimator of transfer function for the base input to isolated mass linear damping experimental (—), cubic damping experimental (—), cubic damping simulation (--)

5. Numerical Simulations and Statistical Analysis

In this section, the response statistics of the system are examined in order to establish the cause of the differing behaviours of the cubically damped system to harmonic and random excitation. Numerical simulations are used given their close agreement with measurements, which allows for longer datasets and better statistical estimates. Simulations were performed by direct numerical integration of Eq. (1) in Matlab using the ODE45 solver. In the case of random excitation the input time histories were generated using the inverse Fourier transform of a band-limited spectrum with constant amplitude R and uniformly distributed random phase ϕ, i.e. $X(f) = Re^{i\phi}$ where R is a real number and $\phi \in [0, 2\pi]$. The spectra of the response variables and associated transfer functions were estimated using the 'pwelch' and 'cpsd' functions in Matlab. The time responses were truncated and windowed using a Hanning window and averaged with an overlap of 75%.

The bandwidth of the displacement input spectrum was varied so as always to span the resonance at 10Hz. The probability density functions (PDFs) for bandwidths of 7-25Hz and 7-100Hz are shown in Fig. 8(a) and (b) respectively. Also shown are the PDFs for a harmonic displacement input of equal rms value (0.025mm and 0.056mm respectively) which, by contrast to the PDFs of the random input, are bounded with high peaks at the amplitude of the harmonic input. The distributions of the predicted relative velocities mirror those of the displacement input for both types of excitation, notwithstanding the nonlinearity of the system. These are represented by the thin solid lines in Fig. 9(a) and (b). Also shown against a secondary *y*-axis in these figures is the damping force as a function of the relative velocity for the value of cubic damping coefficient used, $c_3 = 21\text{kNs}^3/\text{m}^3$. A larger rms relative velocity can be expected to give rise to higher damping forces.

Fig. 10 shows the amplitude ratio for the two bandwidths of random excitation chosen. In contrast to a linearly damped system the response depends on the excitation amplitude. The resonance peak, for example, is nearly 20dB lower for the wider bandwidth due to the five-fold increase in bandwidth and hence rms of the base input. There is some associated detriment in performance above resonance. Also shown are the corresponding results for a harmonic input of the same rms displacement. At the lower excitation level a harmonic input results in a lower resonance peak than random excitation. The peaks in the tails of the PDFs seen in Fig. 9 result in higher damping forces. However, the situation is reversed for a higher level of excitation. The reason for this apparent anomaly is related to the input velocity rather than the input displacement. The amplitude of the harmonic input is chosen such that, at all frequencies, $rms(x_0)$ is equal to that of the random input. However, the rms of the associated velocity input is frequency dependent and is given by $\omega.rms(x_0)$. By contrast the r.m.s of the velocity of the random input is independent of frequency and (when $\omega_{upper} >> \omega_{lower}$) is approximately given by $\frac{1}{\sqrt{3}}\omega_{upper}.rms(x_0)$, where ω_{upper} is the upper frequency of the input spectrum. Consequently, the rms of the harmonic velocity input is significantly lower than that for the random excitation below ω_{upper} and much higher when $\omega >> \omega_{upper}$. The amplitude ratio for harmonic excitation appears more lightly damped but rises steadily towards the corresponding random result at 100Hz. The curve tends to 0dB beyond the frequency range shown. This represents a considerable disadvantage of cubic damping in the case of a harmonic displacement input that is not observed for random excitation and is a manifestation of the assumed constant displacement input. A comparison between harmonic and random excitation in which the rms of the input velocity or acceleration is kept constant can be expected to yield different conclusions.

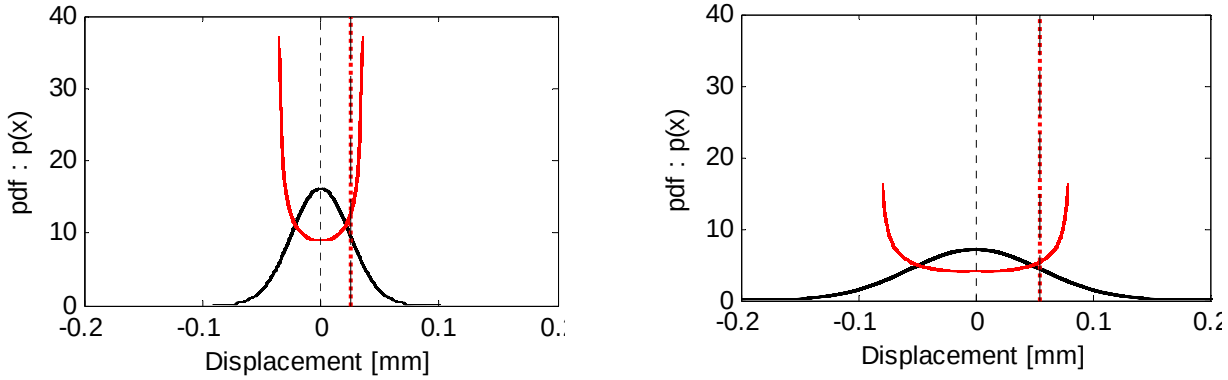

(a) σ_{x_0} = 0.025 mm (7-25Hz random) (b) σ_{x_0} = 0.056 mm (7-100Hz random)

Figure 8. Probability Density Function of displacement input for broadband and harmonic excitation with the same rms value, broadband excitation (—), harmonic excitation (—)

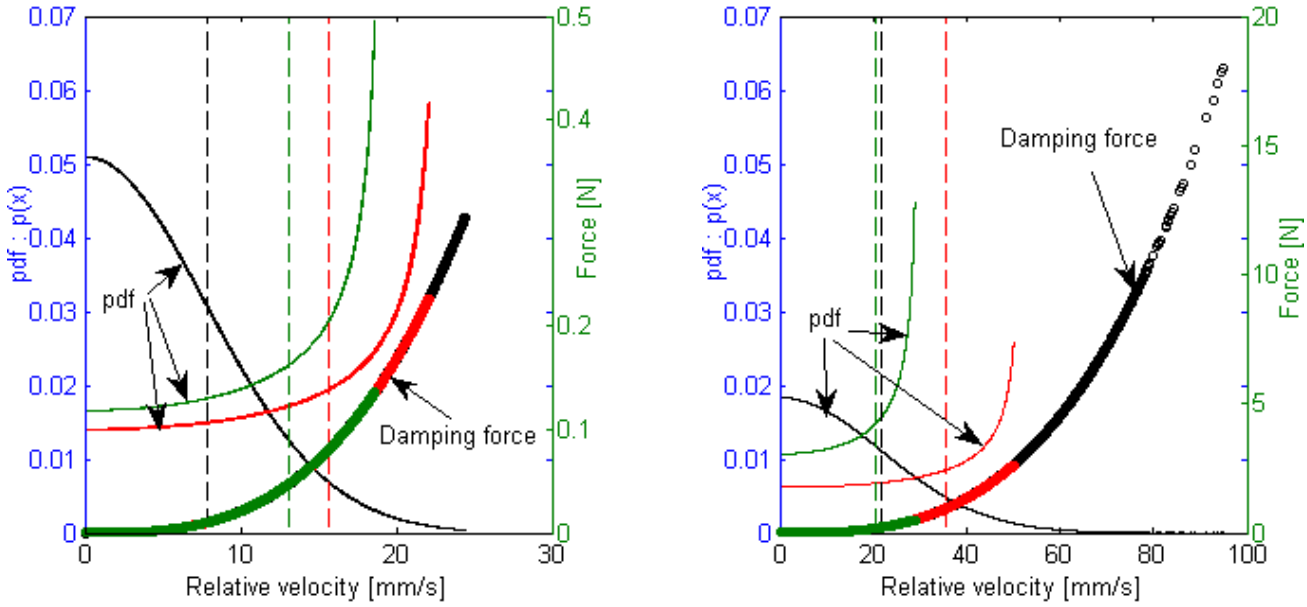

(a) 7-25Hz (σ_{x_0} = 0.025 mm) (b) 7-100Hz (σ_{x_0} = 0.056 mm)

Figure 9. Probability Density Function for relative velocity: random (—), 10Hz harmonic (—), 100Hz harmonic (—), and characteristic diagram (force vs relative velocity). The dashed lines represent the standard deviation of relative velocity in each case.

6. Conclusions

The broadband response for an isolation system with cubic damping has been studied and found to exhibit quite different characteristics compared to the harmonic excitation case. This difference has been confirmed experimentally in which velocity feedback control was used to realise cubic damping actively. Numerical simulations have been performed for random and harmonic base inputs of the same r.m.s values. The results show that the system appears more lightly damped to harmonic than random excitation except at the higher end of the considered bandwidth where they become comparable. At higher frequencies still the cubically damped system tends to a transmissibility of unity for harmonic excitation. However, this is a manifestation of the assumed constant displacement input which is not typical of real life applications.

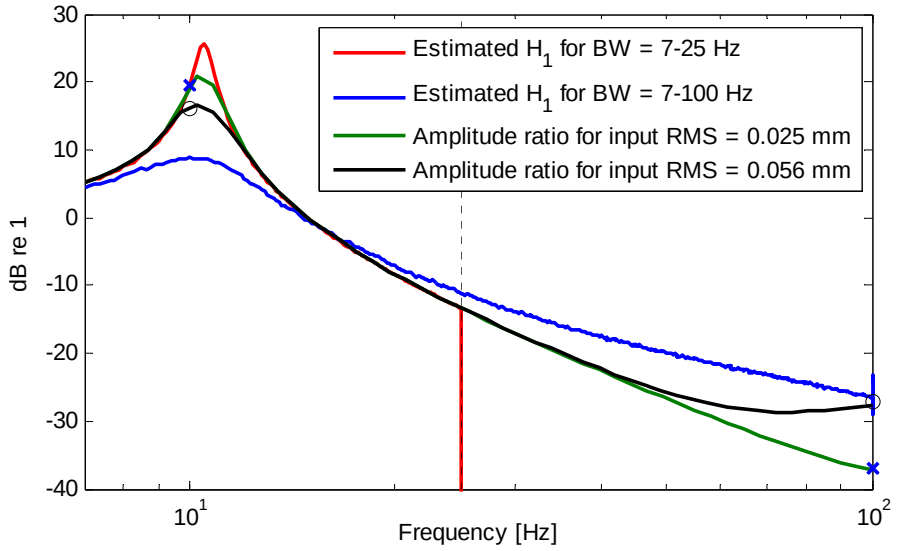

Figure 10. Amplitude ratio for the system with cubic damping subject to a random displacement input of bandwidth 7-25Hz (—) and 7-100Hz (—), and a harmonic displacement input with the same rms value, 0.025mm (—) and 0.056mm (—). The markers indicate the amplitude ratio for a harmonic input at 10Hz and 100Hz, i.e. at frequencies corresponding to Fig. 9.

REFERENCES

1 Jing, X. and Lang, Z., Frequency domain analysis of a dimensionless cubic nonlinear damping system subject to harmonic input, *Nonlinear Dynamics,* **58**(3), pp. 469-485, (2009).

2 Peng, Z. K., Lang, Z. Q., Jing, X. J., Billings, S. A., Tomlinson, G. R. and Guo, L. Z., The transmissibility of vibration isolators with a nonlinear antisymmetric damping characteristic, *Journal of Vibration and Acoustics,* **132**(1), pp. 1-7, (2010).

3 Laalej, H., Lang, Z. Q., Daley, S., Zazas, I., Billings, S. A. and Tomlinson, G. R., Application of non-linear damping to vibration isolation: an experimental study, *Nonlinear Dynamics,* **69**(1-2), pp. 409-421, (2012).

4 Shekhar, C. N., Hatwal, H. and Mallik, A. K., Performance of non-linear isolators and absorbers to shock excitations, *Journal of Sound and Vibration,* **227**(2), pp. 293-307, (1999).

5 Kovačić, I., Milovanović, Z. and Brennan, M. J., On the relative and absolute transmissibility of a vibration isolation system subjected to base exctation, *FACTA UNIVERSITATIS Series: Working and Living Environmental Protection,* **5**(1), pp. 39 - 48, (2008).

6 Milovanovic, Z., Kovacic, I. and Brennan, M. J., On the displacement transmissibility of a base excited viscously damped nonlinear vibration isolator, *Journal of Vibration and Acoustics,* **131**, pp. 1-7, (2009).

7 Panananda, N., Ferguson, N. S. and Waters, T. P., The effect of cubic damping in an automotive vehicle, *Proceeding of the International Symposium on the Computational Modelling and Analysis of Vehicle Body Noise and Vibration*, University of Sussex, Brighton, UK, 27-28 March, (2012).

8 Peng, Z. K., Meng, G., Lang, Z. Q., Zhang, W. M. and Chu, F. L., Study of the effects of cubic nonlinear damping on vibration isolations using Harmonic Balance Method, *International Journal of Non-Linear Mechanics,* **47**(10), pp. 1073-1080, (2012).

9 Panananda, N., Ferguson, N. S. and Waters, T. P., The effect of cubic damping on a base excited isolator: an experimental study for harmonic excitation, *Proceedings of the 11th International Conference on Recent Advances in Structural Dynamics (RASD)*, University of Pisa, Italy, 1-3 July, (2013).